Polym. Bull. (2011) 67:1785–1797
DOI 10.1007/s00289-011-0506-z

ORIGINAL PAPER

Enhanced interfacial interaction for effective reinforcement of poly(vinyl alcohol) nanocomposites at low loading of graphene

Xiaoya Yuan

Received: 8 February 2011 / Revised: 13 May 2011 / Accepted: 15 May 2011 /
Published online: 21 May 2011

Abstract The graphene/poly(vinyl alcohol) (PVA) nancomposites with homogeneous dispersion of the nanosheet and enhanced nanofiller–matrix interfacial interaction were fabricated via water blending partially reduced graphene oxide and PVA. The nanocomposites were characterized by X-ray diffraction, Fourier transform infrared spectroscopy, scanning electron microscopy, and thermogravimetry. The graphene nanosheets were fully exfoliated in the PVA matrix and a new covalent linkage was formed between graphene and PVA matrix. Uncommon to conventional method, the enhanced interfacial adhesion resulted from covalent interaction and hydrogen bondings between graphene and PVA backbone. The mechanical and thermal properties of the nanocomposites were significantly improved at low graphene loadings. An 116% increase in tensile strength and a 19 °C improvement of onset thermal degradation temperature were achieved by the addition of only 0.8 wt% graphene.

Keywords Graphene · Poly(vinyl alcohol) · Nanocomposites · Interfacial interaction · Mechanical property · Thermal property

Introduction

Graphene is an atom thick, two-dimensional planar sheet composed of sp^2-hybridized carbon atoms arranged in a honeycomb lattice and has been viewed as the building block for other carbon allotropes of different dimensionality [1–3]. It has attracted tremendous attention from the experimental and theoretical scientific communities in recent years due to its unique mechanical and physical properties [4–6]. The extraordinary Young's modulus (~1.0 TPa) and fracture strength

X. Yuan (✉)
College of Science, Chongqing Jiaotong University, Chongqing 400074, People's Republic of China
e-mail: yuanxy@cquc.edu.cn

($\sim$125 GPa) [7], large theoretical specific surface area ($\sim$2,630 $m^2\ g^{-1}$) [8], high intrinsic mobility ($\sim$200,000 $cm^2\ V^{-1}\ s^{-1}$) [9], and thermal conductivity ($\sim$5,000 $W\ m^{-1}\ K^{-1}$) [10] make graphene a promising nanofiller to improve mechanical, electrical, thermal, and gas barrier properties of polymers [11–15]. Compared to conventional micro- or nano-scale fillers, graphene can be obtained at lower cost from graphite through different methods [16, 17] and graphene-based polymer nanocomposites (GPN) can be also prepared by the standard routes such as melt blending [18, 19], solution mixing [20–22], in situ covalent reaction or intercalative polymerization [23–25], spin casting [26, 27], and self-assembly [28] to yield molded products with reasonable shelf [29]. Furthermore, graphene or graphene-derived materials out-perform the other fillers as an additive in many cases and have exhibited dramatic improvements in polymer properties due to the large surface area and high aspect ratio of these materials at lower loading of graphene [14, 15, 29]. Chen and coworkers [30] demonstrated a solution-processed poly(vinyl alcohol) (PVA)–graphene oxide (GO) nanocomposites and a 76% increase in tensile strength and 62% improvement of Young's modulus were achieved at only 0.7 wt% of GO. Koratkar compared reinforcement efficiency of graphene with single- or multi-walled carbon nanotube (CNT) and the superiority of graphene platelets over CNT was fully exemplified at a nanofiller weight fraction of 0.1–0.002% [20].

However, it is not quite ready to develop the GPN, especially with graphene as the reinforcement filler. Before achieving high performance of GPNs, it must be considered: (a) homogeneous dispersion or full exfoliation of graphene sheets in polymer matrix, and (b) strong interfacial interaction between the nanosheets and the surrounding polymer host, which is responsible for the effective transfer of external load. Because of the high specific surface area and van der Waals interaction between the interlayers of graphene sheets, graphene tends to form irreversible agglomerates or even restack, which lowers its effectiveness as a nanofiller for reinforcement. Much of current research are focused on dispersion improvement and many methods have been developed such as functionalization of graphene nanosheets to compatibilize the nanofiller with the matrix [31], blending with polymers prior to the chemical reduction of GO [32], in situ intercalative polymerization of monomer [33], and so on. In fact, individual graphene sheet does not contain any of functional groups on its surface, while those directly prepared by chemical or thermal reduction of GO bear little functional groups [17], which is not enough to produce strong interfacial adhesion between the nanosheet and polymer matrix. Therefore, how to exert the graphene's reinforcement via the strong interfacial adhesion and the transfer of its excellent mechanical property to the polymer matrix in the nanocomposites is very urgent [34]. Up to date, few works has concerned the interfacial interaction between graphene sheets and polymer matrix in GNPs [30]. GO, which contains various oxygen functional groups on their basal planes and edges, is hydrophilic and can be easily dispersed as individual sheets in polar solvents to form a stable suspension and graphene/polymer composites are subsequently produced after the reduction of GO [35], where the nanosheet can be completely exfoliated and homogeneous dispersed in the matrix. Whereas, it is necessary to increase the amount of functional groups on the surface

of graphene sheets to enhance the interfacial interaction between graphene sheets and polymer matrix for reinforcement improvement. To the best of our knowledge, the most effective approach is to use chemical bond between the filler and polymer matrix. Based on these considerations, in this manuscript, the soluble polymer PVA was chosen and partially reduced graphene oxide (PRGO) was prepared by controlled chemical reduction, where a few oxygenated functional groups were preserved for covalent bonding. The graphene/PVA nanocomposites were then prepared via a solution blending using water as the processing solvent. Interfacial interaction was dramatically enhanced due to chemical linkage and hydrogen bondings between graphene and PVA backbone, which favored an improvement in thermal and mechanical properties of the nanocomposites.

Experimental

Materials

Natural graphite flakes with an average particle size of 150 μm and a purity of >98% were supplied from Qingdao Nanshu Graphite Co., Ltd. Potassium hydroxide was purchased from Chongqing Chuandong Chemicals (Chongqing, China). Hydrazine hydrate (85%) was provided from Sinopharm Chemical Reagent Co., Ltd. PVA ($M_w \approx$ 10,000, 99% hydrolyzed) was obtained from Yunnan Yunwei Co., Ltd. All the materials were used as received and without further purification.

Preparation of partially reduced graphene oxide

PRGO was synthesized through chemical reaction of GO colloids with KOH at pH 10.6 and then reduction with hydrazine according to Ruoff's method [36]. The typical synthesis procedure of PRGO was described as follows: GO, used as the starting material, was synthesized from natural graphite flakes using a modified Hummers method [37, 38]. After being purified by several runs of centrifugation/washing to completely remove residual salts and acids, GO was dispersed in water and then ultrasonicated for 30 min with a ultrasonic cleaner (As2060B, Automatic Science Instrument Co. Ltd.) leading to colloidal suspension of an exfoliated GO sheets. KOH aqueous solution was added to the as-prepared GO suspension to adjust pH 10.6. After stirring for 2 h at room temperature, the dispersion was then subjected to post-reduction by hydrazine monohydrate (hydrazine: GO = 1:8 in weight) at ca. 95 °C for 1 h, which gave a black suspension. The as-obtained suspension was then centrifugated to afford PRGO powder. The separated PRGO was washed with water several times and dried under vacuum for 12 h.

Preparation of graphene/PVA nanocomposites

The synthesis procedure for a typical graphene/PVA nanocomposite with graphene loading of 1.0 wt% was as follows: PRGO (100 mg) was suspended in deionized water (100 mL) and ultrasonicated for 10 min to afford uniform graphene solution.

PVA (10.0 g) was dissolved in distilled water (200 mL) and heated to 90 °C. When PVA was completely dissolved, the as-prepared graphene solution was gradually added and the mixture was stirred for addition 2 h at 90 °C. Finally, this homogeneous graphene/PVA solution was poured into an aluminum pan and kept in vacuum at 60 °C to form a graphene/PVA composite film, until the weight reached an equilibrium value. This film was peeled off from the substrate for mechanical testing. A series of graphene/PVA nanocomposites with graphene loadings of 0.4, 0.6, 0.8, and 1.0 wt% were similarly prepared.

Characterization

FTIR was measured on Nicolet 6700 Fourier Transform Infrared instrument with scanning from 400 to 4000 cm^{-1} by using KBr disks. The UV–vis absorption spectra were measured on a Lambda 35 (Perkin-Elmer) spectrophotometer. Transmission electron microscopy (TEM) was performed using a JEM-200CX electron microscope at an acceleration voltage of 200 kV. The sample solution was dropped onto carbon-coated copper grids (mesh size 300) and allowed to dry under ambient conditions. Scanning electron microscopy (SEM) was performed on a FEINova 400 Nano scanning electron microscope with acceleration voltage of 20 kV. Samples were prepared by immersing the films in liquid nitrogen for 10 min before fracture. The fracture surfaces were coated with gold before analysis. X-ray diffraction (XRD) measurements were carried out using a Rigaku D/Max-2500 diffractometer with Cu K_α radiation. Thermogravimetric analysis (TGA) was performed with Netzsch STA 449C thermogravimetric analyzer under nitrogen atmosphere at a heating rate of 10 °C/min and approximately 10 mg of each sample were measured under N_2. The mechanical properties of the graphene/PVA nanocomposites were measured by a universal tensile testing machine (SANS Co., Ltd, China) at room temperature according to ASTM D882-2009.

Results and discussion

Preparation of PRGO

PRGO was prepared via chemical reaction of GO colloids with KOH and consequent reduction with hydrazine according to reported method [36]. After adding KOH to the aqueous suspension of GO, the reaction between KOH and oxygen functional groups such as carboxylic acid, hydroxyl and epoxy groups in the GO sheets occurred, leading to large negative charges and strong interaction of K^+ with oxygenated groups in the GO sheets, which could be stable against chemical reduction by hydrazine. During the process of hydrazine reduction, the yellow–brown color of GO solution gradually changed to black and the reaction was monitored by UV–vis spectroscopy. Figure 1 shows the UV–vis spectra of GO and PRGO. For GO solution, a maximum peak at 235 nm was ascribed to $\pi \rightarrow \pi^*$ transition of aromatic C–C bonds, and a shoulder at 300 nm attributed to $n \rightarrow \pi^*$ transition of C=O bonds. In the case of PRGO, after reduction the maximum peak

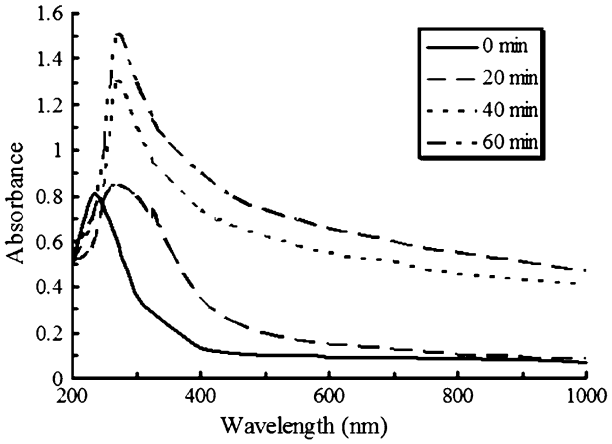

Fig. 1 UV–Vis spectra monitoring the reduction of GO solution as a function of reaction time

was red-shifted to 270 nm and the absorbance was significantly increased in the whole spectra region ($\lambda > 230$ nm), which indicated that electronic conjugation within the graphene sheets has been restored. Little increase in the absorption was found after 1 h, suggesting completion of the reduction within that period. Furthermore, the surface of PRGO in the aqueous solution should still be negative charged and the electrostatic repulsion enabled the formation of well-dispersed exfoliated PRGO colloids in water, which could be confirmed by TEM measurements. As shown in Fig. 2, PRGO was fully exfoliated into individual sheets by ultrasonic treatment. These results indicated that, similar to the original GO dispersion, the as-prepared PRGO sheets remained separated in the water dispersion.

Figure 3 shows the FTIR spectra of pristine graphite, GO, and the as-prepared PRGO. Compared to few characteristic absorption in the spectrum of pristine graphite, a strong and broad absorption in the range of 3400–3500 cm^{-1} due to O–H stretching vibration and the peak at 1730 cm^{-1} related to the C=O stretching of

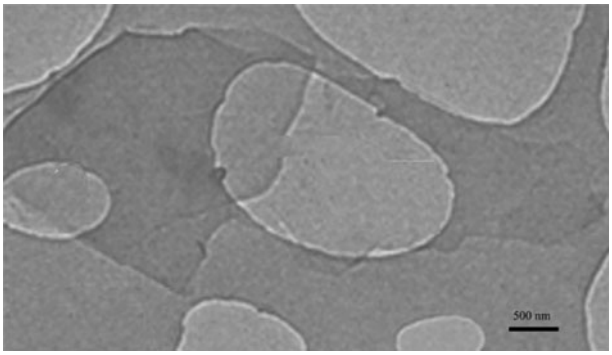

Fig. 2 A typical TEM image of PRGO nanosheet in an aqueous solution

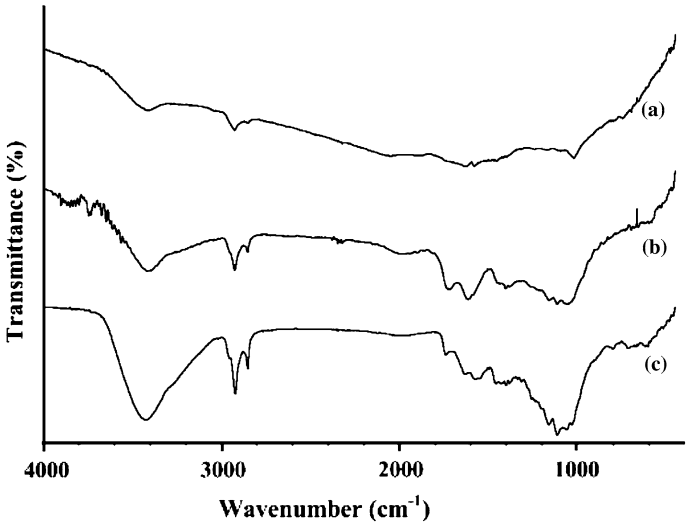

Fig. 3 FTIR spectra of pristine graphite (*a*), GO (*b*), and PRGO (*c*)

carboxylic groups situated at edges of GO sheets were observed. However, the C=O peak intensity at 1730 cm^{-1} was significantly weaken in the spectrum of PRGO (Fig. 3c), suggesting K^+-modified oxygenated groups (e.g., carboxylic acid and phenol hydroxyl) was still remained in the reduced product PRGO after chemical reduction of GO [36]. The absorption assigned to the O–H bending vibration was also detected around 1621 cm^{-1} in the spectrum of PRGO. The C/O atomic ratio of GO, PRGO, and highly reduced GO [39] was further investigated by elemental analysis. The C/O atomic ratio of PRGO (3.6), interspaced GO (2.1), and highly reduced GO (9.8), showing PRGO contained more O atoms than the highly reduced GO after control reduction of GO although a combination of trapped water between graphene sheets and the oxygen functional groups on the sheets should be considered. The IR spectrum of PRGO and elemental analysis confirmed the existence of oxygen functionalities located presumably at the edges of graphene sheets [40]. These oxygen functionalities rendered PRGO hydrophilic and water processable, so that the as-prepared PRGO could be exfoliated and intercalated by other hydrophilic molecules to form stable colloids or to produce polymer nanocomposites [14, 15].

Morphology and structure of nanocomposites

The homogeneous dispersion of the nanosheets in the matrix is very crucial to improve the mechanical property of the GPNs. To well-disperse the graphene sheets into the polymer, PRGO was first exfoliated in water and water-soluble PVA was then added. After solution blending of PRGO and PVA at higher temperature and subsequent vacuum-evaporation of the solvent, the graphene/PVA nanocomposites were obtained and the morphology and structure of the as-prepared products were

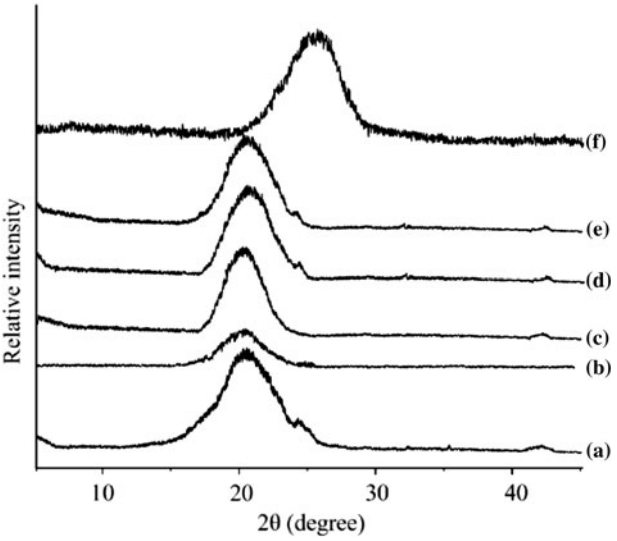

Fig. 4 XRD patterns of pure PVA (*a*), graphene/PVA nanocomposites with graphene loading of 0.4 wt% (*b*), 0.6 wt% (*c*), 0.8 wt% (*d*), 1.0 wt% (*e*), and PRGO (*f*)

probed by XRD and SEM. XRD is an important tool to determining whether graphene-based sheets are indeed present as individual sheets in the nanocomposites. Figure 4 shows the XRD patterns of pure PVA, graphene/PVA nanocomposite with different loading graphene. The PRGO nanosheets showed a typical broad diffraction peak at $2\theta = 25°$, consistent with previous reports for graphene nanosheets obtained from chemical reduction of GO [30, 32]. Pure PVA also exhibited a characteristic peaks of PVA at $2\theta = 20.5°$. However, as dispersing the graphene nanosheets into the PVA matrix, the broad peak of graphene disappeared in the composites and only a single diffraction peak around 20° arisen from PVA was detected, suggesting the disorder of graphene and intercalation of PVA into inter-layers of graphene [32]. The XRD results clearly indicated that PRGO was fully exfoliated into individual graphene sheets and dispersed at the molecular level into the PVA matrix.

Figure 5 displays the SEM image of the cross-section of the nanocomposite with graphene loading of 0.8 wt%. It could be easily seen that most of the graphene nanosheets were intercalated by PVA upon solution blending and well-exfoliated in the nanocomposite, forming a homogeneous dispersion of the nanofiller in the polymer matrix. The image also disclosed the graphene nanosheets randomly dispersed and somewhat wrinkled and crumpled, not parallel with each other, which could be attributed to much extent to strong interaction between the main chain of PVA and oxygen functionalities on the surface of PRGO. This phenomenon was also mentioned elsewhere [20, 41] and should contribute to enhance the mechanical property of graphene/PVA nanocomposites.

Aqueous PVA solution is a colloidal suspension and the pendant hydroxyl groups become ready acceptors for hydrogen bonding, which increases its interaction with

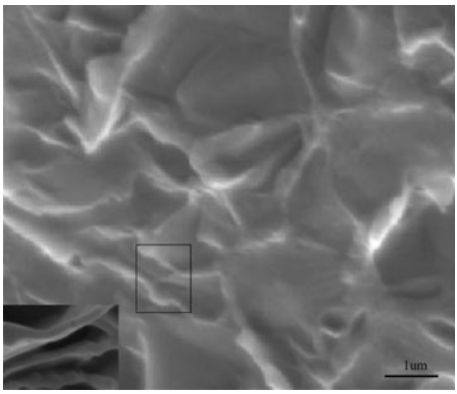

Fig. 5 SEM image of cross-section of the graphene/PVA nanocomposite with graphene loading of 0.8 wt%. The inset showing the rectangular region with a high magnification

the water molecules and makes PVA soluble in water. Hydroxyl groups of PVA can also form strong hydrogen bonds with hydroxyl and carboxyl groups present on PRGO [30]. Furthermore, chemical reactions between the PVA and oxygen functionalities on the surface of PRGO could also occur upon heating [42], leading to the formation of new ester group in the nanocomposites. As a consequence, hydrogen bonds and the new covalent bond should enhance the interfacial interaction between PVA and graphene, which favored property improvements with graphene as the reinforcement nanofiller. FTIR was used to monitor the process between PVA and PRGO at higher temperature. To ensure no traces of non-reacted PRGO remained in the nanocomposites, purification of the products was achieved by high-speed centrifugation. As shown in Fig. 6, compared to that of PVA, the FTIR spectra of graphene/PVA retained most of the bands of PVA, although some of them changed in intensity and showed new bands. The new absorption in FTIR spectra of the

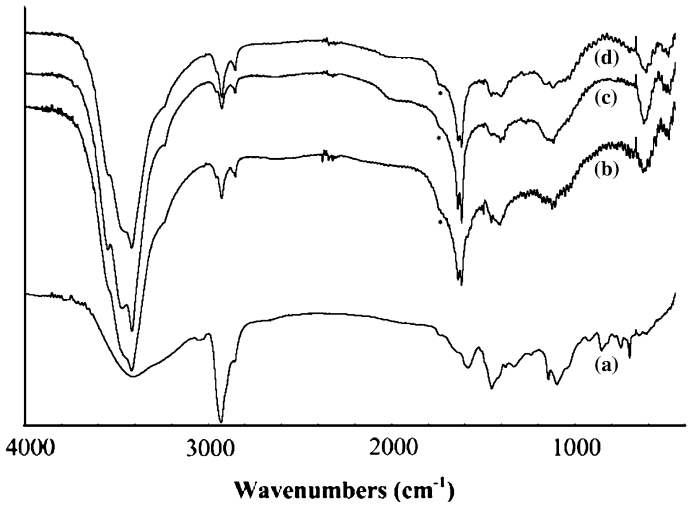

Fig. 6 The FTIR spectra of PVA (*a*) and its nanocomposites with graphene loading of 0.6 wt% (*b*), 0.8 wt% (*c*), and 1.0 wt% (*d*). The *asterisk* denotes the peak at 1740 cm^{-1}

nanocomposites around 1740 and 1620 cm^{-1} could be attributed to C=O stretching of ester linkage and the skeletal vibration of non-oxidized graphitic domains, respectively, Notably, PVA also exhibited an absorption at 1730 cm^{-1} due to incomplete hydrolysis of the raw material. However, the absorption at 1740 cm^{-1} became stronger with an increase of graphene loading, suggesting esterification reaction of PVA and carboxylic acid on the PRGO occured and the graphene nanosheets were grafted onto PVA in our system. The C=O absorption appeared weak presumably due to low amount of functional groups on PRGO and subsequently low degree of esterification [43]. However, there was somewhat stronger absorption peak at 1100 cm^{-1}, which was assigned as the absorption peak of C–O–C group. Moreover, the intense band at 3000–3600 cm^{-1} due to hydroxyl groups of polymeric unit became wider as increasing graphene content and this indicated van der Waals forces and hydrogen-bond interactions between PVA and graphene.

Thermal and mechanical properties of graphene/PVA nanocomposites

It is expected that thermal and mechanical properties of the as-prepared graphene/PVA nanocomposites can be significantly enhanced, largely by the large interfacial area and high aspect ratio of the nanosheet, the molecular dispersion of the graphene sheets in the matrix, and strong adhesion between graphene and PVA due to hydrogen bonding and covalent linkage. The representative stress–strain curves for graphene/PVA nanocomposites with different graphene loadings are presented in Fig. 7. It is obvious that the addition of graphene into the polymer matrix has a significant influence on the mechanical behavior. Upon the graphene nanosheet loading, the mechanical performance of the graphene/PVA nanocomposite was dramatically increased as compared to that of pure PVA matrix. With only 0.8 wt% graphene, the tensile strength of the nanocomposite was up to 69 MPa while that of

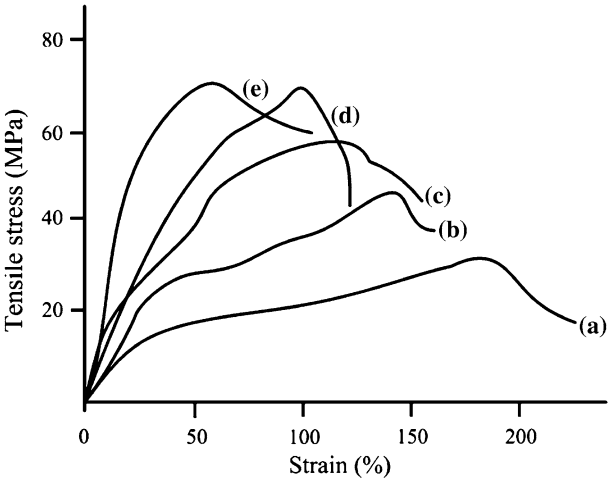

Fig. 7 Representative stress–strain curves of graphene/PVA nanocomposites with various graphene loadings of 0 wt% (*a*), 0.4 wt% (*b*), 0.6 wt% (*c*), 0.8 wt% (*d*), and 1.0 wt% (*e*)

the PVA parallel sample was 32 MPa; i.e., the tensile strength increased by 116%. The increasing trend was especially clear with lower loading. For example, the addition of 0.6 wt% graphene into the matrix increased the tensile strength by 81% from 32 to 58 MPa. The strength reinforcement at low graphene content was more obvious than those reported in similar graphene- or GO-reinforced composites [30, 44, 45]. However, while further increasing graphene loading from 0.8 to 1.0 wt%, the tensile strength increased slightly from 69 to 71 MPa without a pronounced change and this implied there existed a mechanical percolation probably due to the nanosheet restacking in the case of higher graphene content, which was consistent with the results of Zhao et al. [32]. On the contrary, as shown in Fig. 8, the elongation at break of the nanocomposites gradually decreased as compared to pure PVA. The value of the elongation at break decreases from 225% for pure PVA sample to 58% for the nanocomposite with 1.0 wt% loading. The mechanical reinforcement with graphene was believed to effective interfacial load transfer due to enhanced nanofiller–matrix adhesion between graphene and PVA matrix [34]. Meanwhile, the composites became somewhat black with graphene loading as presented in Fig. 9 (the black spot was introduced during molding, not the carbon agglomerates), which probably limited their potential use.

TGA was also conducted to investigate the effect of graphene nanosheets on the thermal behavior of polymer matrix. Figure 10 displays TGA and corresponding differential thermogravimetric (DTG) thermograms for pure PVA and graphene/PVA nanocomposite with 0.8 wt% graphene loading. Both pure PVA and its nanocomposite exhibited a two-step degradation behavior with different thresholds. The first step at about 200–350 °C was considered the thermal decomposition of PVA and the second weight loss step at about 400–520 °C should be of the residue. Compared to that of pure PVA, the TGA curve of the nanocomposite was shifted toward higher temperature and the onset temperature of thermal degradation for the nanocomposite with graphene loading of 0.8 wt% was significantly increased from

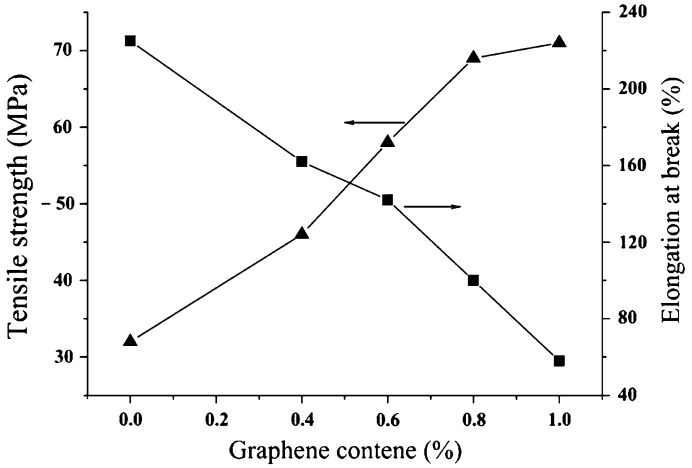

Fig. 8 Mechanical properties of graphene/PVA nanocomposites with various graphene loadings: tensile strength (*left*) and elongation at break (*right*) versus graphene loadings

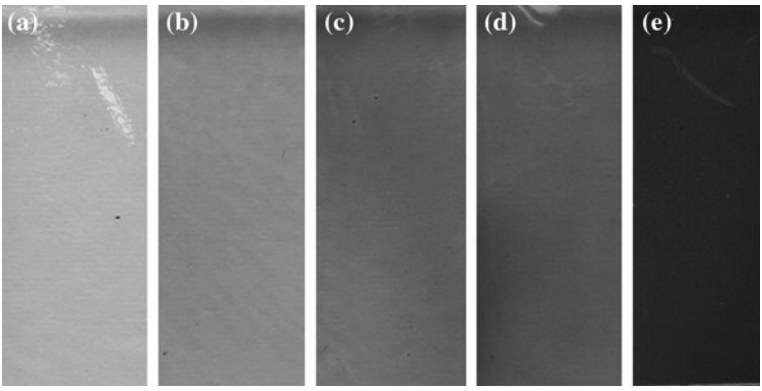

Fig. 9 Optical image of PVA–graphene nanocomposite films with various graphene loadings of 0 wt% (**a**), 0.4 wt% (**b**), 0.6 wt% (**c**), 0.8 wt% (**d**), and 1.0 wt% (**e**)

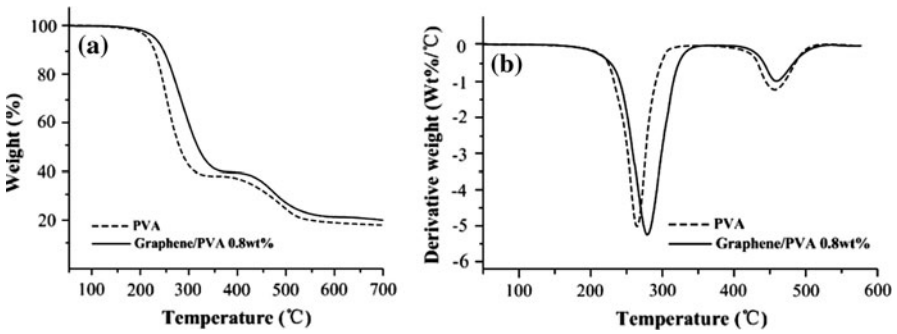

Fig. 10 TGA (**a**) and DTG (**b**) curves of pure PVA and graphene/PVA nanocomposite with graphene loading of 0.8 wt%

210 for pure PLA to 229 °C. The peak decomposition temperature of the DTG curve represents the temperature at which the maximum weight loss rate was reached, as shown in Fig. 10b. The peak decomposition temperature of the nanocomposite appeared at about 280 °C and was increased by about 15 °C compared to that of pure PVA. The increased value was much higher than that of similar graphene/PVA nanocomposites [30, 44], largely due to more oxygen functionalities on the surface of graphene. These results indicated that addition of functional graphene at a low loading improved significantly the thermal stability of the nanocomposite, which could be reasonably explained by enhanced interfacial interaction between graphene nanosheets and PVA matrix.

Conclusion

In conclusion, the graphene/PVA nancomposites with homogeneous dispersion of the nanosheet and enhanced nanofiller–matrix interfacial interaction were fabricated

via a simple solution-blending method. In our system, new covalent linkage was formed between graphene and PVA matrix and the nanocomposites displayed strong interactions among the polymer and nanosheets due to the covalent adhesion and hydrogen bonding. Significant enhancement of thermal and mechanical properties of graphene/PVA nanocomposites was obtained at fairly low loadings of graphene. The facile method presented here could be extended to the implementation of other graphene-based polymer nanocomposites. Because of the easy preparation of functionalized graphene nanosheets, graphene as an effective nanofiller could be used for many practical applications.

Acknowledgments The authors would like to gratefully acknowledge the supports by Municipal Science Foundation Project of CQ CSTC (No. 2007BB4442)and of CQEC (No. KJ070402) and Open-end Fund of Hi-tech Lab for Mountain Road Construction and Maintenance, CQTJU (CQMRCM-10-5).

References

1. Novoselov KS, Geim AK, Morozov SV, Jiang D, Zhang Y, Dubonos SV, Grigorieva IV, Firsov AA (2004) Electric field effect in atomically thin carbon films. Science 306:666–669
2. Geim AK, Novoselov KS (2007) The rise of graphene. Nat Mater 6:183–191
3. Geim AK (2009) Graphene: status and prospects. Science 324:1530–1534
4. Allen MJ, Tung VC, Kaner RB (2010) Honeycomb carbon: a review of graphene. Chem Rev 110:132–145
5. Rao CNR, Sood AK, Voggu R et al (2010) Some novel attributes of graphene. J Phys Chem Lett 1:572–580
6. Kim J, Kim F, Huang J (2010) Seeing graphene-based sheets. Mater Today 13:28–38
7. Lee CG, Wei XD, Kysar JW, Hone J (2008) Measurement of the elastic properties and intrinsic strength of monolayer graphene. Science 321:385–388
8. Chae HK, Siberio-Perez DY, Kim J (2004) A route to high surface area, porosity and inclusion of large molecules in crystals. Nature 427:523–527
9. Bolotin KI, Sikes KJ, Jiang Z, Klima M, Fudenberg G, Hone J, Kim P (2008) Ultrahigh electron mobility in suspended graphene. Solid State Commun 146:351–355
10. Balandin AA, Ghosh S, Bao WZ, Caliza I, Teweldebrhan D, Miao F, Lau CN (2008) Superior thermal conductivity of single-layer graphene. Nano Lett 8:902–907
11. Wu JS, Pisula W, Mullen K (2007) Graphenes as potential material for electronics. Chem Rev 107:718–747
12. Stankovich S, Dikin DA, Dommett GHB, Kohlhaas KM, Zimney EJ, Stach EA, Piner RD, Nguyen ST, Ruoff RS (2006) Graphene-based composite materials. Nature 442:282–286
13. Arora A, Padua GW (2010) Nanocomposites in food packing. J Food Sci 75:R43–R49
14. Kim H, Abdala AA, Macosko CW (2010) Graphene/polymer nanocomposites. Macromolecules 43:6515–6530
15. Kuila T, Bhadra S, Yao D, Kim NH, Bose S, Lee JH (2010) Recent advances in graphene based polymer composites. Prog Polym Sci 35:1350–1375
16. Park R, Ruoff RS (2009) Chemical methods for the production of graphenes. Nat Nanotechnol 4:217–224
17. Loh KP, Bao Q, Ang PK et al (2010) The chemistry of graphene. J Mater Chem 20:2277–2289
18. Kim H, Macosko CW (2009) Processing–property relationships of polycarbonate/graphene composites. Polymer 50:3797–3809
19. Zhang HB, Zheng WG, Yan Q, Yang Y, Wang J, Lu Z, Ji GY, Yu Z (2010) Electrically conductive polyethylene terephthalate/graphene nanocomposites prepared by melt compounding. Polymer 51:1191–1196
20. Rafiee MA, Rafiee J, Wang Z, Song H, Yu Z, Koratkar N (2009) Enhanced mechanical properties of nanocomposites at low graphene content. ACS Nano 3:3884–3890

21. Yang Z, Shi X, Yuan J, Pu H, Liu Y (2010) Preparation of poly(3-hexylthiophene)/graphene nanocomposite via in situ reduction of modified graphite oxide sheets. Appl Surf Sci 257:138–142
22. Ansari S, Giannells EP (2009) Functionalized graphene sheet-poly(vinylidene fluoride) conductive nanocomposites. J Polym Sci B 47:888–897
23. Park S, Mohanty N, Suk JW, Nagaraja A, An J, Piner RD, Cai W, Dreyer DR, Berry V, Ruoff RS (2010) Biocompatible, robust free-standing paper composed of a TWEEN/graphene composite. Adv Mater 22:1–5
24. Liu J, Yang W, Tao L, Li D, Boyer C, Davis TP (2010) Thermosensitive graphene nanocomposites formed using pyrene-terminal polymers made by RAFT polymerization. J Polym Sci A 48:425–433
25. Cuong TV, Pham VH, Tran QT, Hahn SH, Chung JS, Shin EW, Kim EJ (2010) Photoluminescence and Raman studies of graphene thin films prepared by reduction of graphene oxide. Mater Lett 64:399–401
26. Xu Y, Long G, Huang L, Huang Y, Wan X, Ma Y, Chen Y (2010) Polymer photovoltaic devices with transparent graphene electrodes produced by spin-casting. Carbon 48:3293–3311
27. Bao Q, Zhang H, Yang JX, Wang S, Tang DY, Jose R, Ramakrishna S, Lim CT, Loh KP (2010) Graphene-polymer nanofiber membrane for ultrafast photonics. Adv Funct Mater 20:782–791
28. Liu J, Tao L, Yang W, Li D, Boyer C, Wuhrer R, Braet F, Davis TP (2010) Synthesis, characterization, and multilayer assembly of pH sensitive graphene–polymer nanocomposites. Langmuir 26:10068–10075
29. Zhu Y, Murali S, Cai W, Li X, Suk JW, Potts JR, Ruoff RS (2010) Graphene and graphene oxide: synthesis, properties, and applications. Adv Mater 22:3906–3924
30. Liang J, Huang Y, Zhang L, Wang Y, Ma Y, Guo T, Chen Y (2009) Molecular-level dispersion of graphene into poly(vinyl alcohol) and effective reinforcement of their nanocomposites. Adv Funct Mater 19:1–6
31. Cao Y, Feng J, Wu P (2010) Alkyl-functionalized graphene nanosheets with improved Lipophilicity. Carbon 48:1670–1692
32. Zhao X, Zhang Q, Chen D, Lu P (2010) Enhanced mechanical properties of graphene-based poly(vinyl alcohol) composites. Macromolecules 43:2357–2363
33. Wang S, Tambraparni M, Qiu J, Tipton J, Dean D (2009) Thermal expansion of graphene composites. Macromolecules 42:5251–5255
34. Gong L, Kinloch IA, Young RJ, Riaz I, Jalil R, Novoselov KS (2010) Interfacial stress transfer in a graphene monolayer nanocomposite. Adv Mater 22:2694–2697
35. Dreyer DR, Park S, Bielawski CW, Ruoff RS (2010) The chemistry of graphene oxide. Chem Soc Rev 39:228–240
36. Park S, An J, Piner RD, Jung I, Yang D, Velamakanni A, Nguyen ST, Ruoff RS (2008) Aqueous suspension and characterization of chemically modified graphene sheets. Chem Mater 20:6592–6594
37. Hummers WS, Offeman RE (1958) Preparation of graphite oxide. J Am Chem Soc 80:1339
38. Gao J, Liu F, Liu Y, Ma N, Wang Z, Zhang X (2010) Environment-friendly method to produce graphene that employs vitamin C and amino acid. Chem Mater 22:2213–2218
39. Stankovich S, Dikin DA, Piner RD, Kohlhaas KA, Kleinhammes A, Jia Y, Wu Y, Nguyen ST, Ruoff RS (2007) Synthesis of graphene-based nanosheets via chemical reduction of exfoliated graphite oxide. Carbon 45:1558–1565
40. Li D, Muller MB, Gilje S, Kaner RB, Wallace GG (2008) Processable aqueous dispersions of graphene nanosheets. Nat Nanotechnol 3:101–105
41. Steurer P, Wissert R, Thomann R, Mülhaupt R (2009) Functionalized graphenes and thermoplastic nanocomposites based upon expanded graphite oxide. Macromol Rapid Commun 30:316–327
42. Sridhar V, Oh I (2010) A coagulation technique for purification of graphene sheets with graphene-reinforced PVA hydrogel as byproduct. J Colloid Interface Sci 348:384–387
43. Salavagione HJ, Gómez MA, Martínez G (2009) Polymeric modification of graphene through esterification of graphite oxide and poly(vinyl alcohol). Macromolecules 42:6331–6334
44. Jiang L, Shen XP, Wu JL, Shen KC (2010) Preparation and characterization of graphene/poly(vinyl alcohol) nanocomposites. J Appl Polym Sci 118:275–279
45. Xu Y, Hong W, Bai H, Li C, Shi G (2009) Strong and ductile poly(vinyl alcohol)/graphene oxide composite films with a layered structure. Carbon 47:3538–3543